Supplementary Material

A synthesis of the upper Arctic Ocean circulation during 2000–2019: Understanding the roles of wind forcing and sea ice decline

Qiang Wang and Sergey Danilov

SUPPLEMENTARY FIGURES

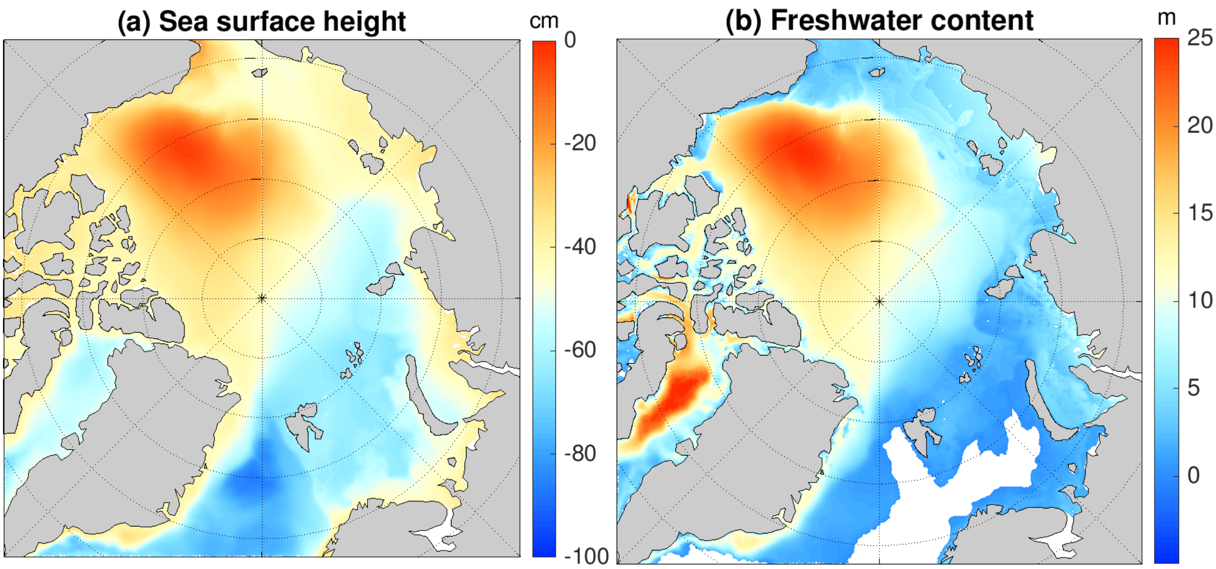

Figure S1. (a) Sea surface height (SSH) and (b) liquid freshwater content (FWC) averaged over 2000-2019 in the FESOM historical simulation. In the Arctic deep basin area the SSH pattern is determined by the FWC pattern.

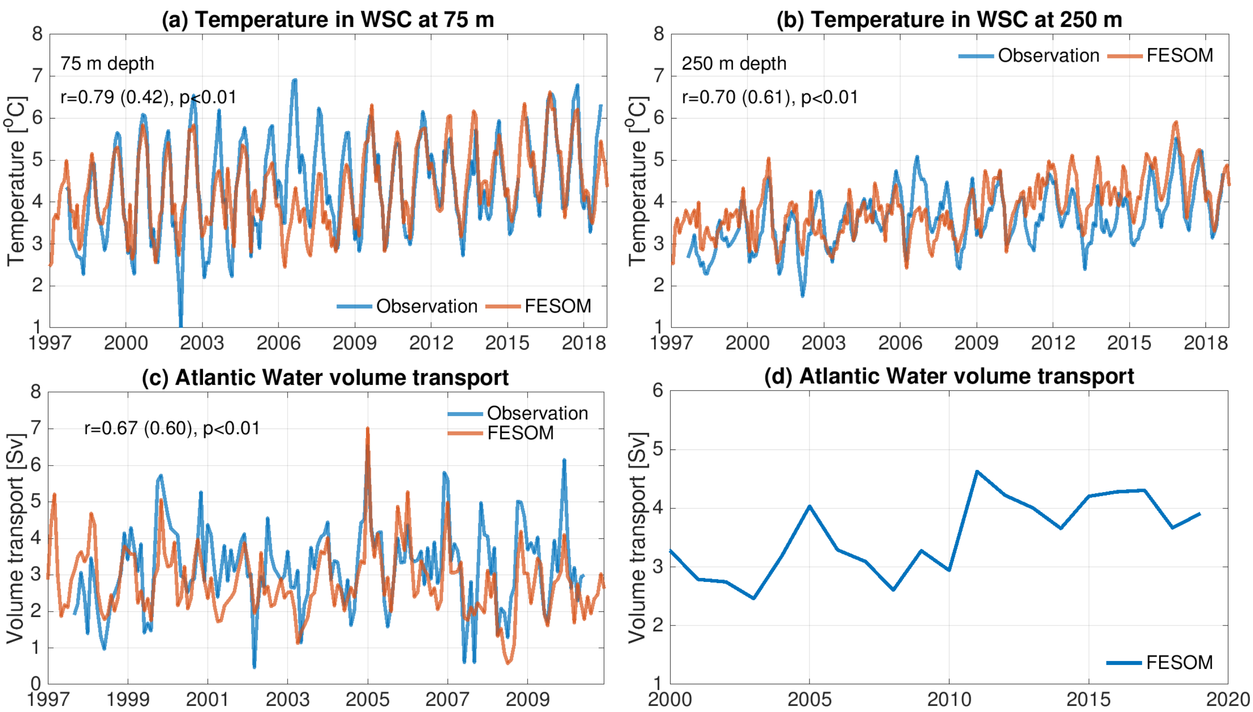

Figure S2. (a)(b) Temperature in the West Spitsbergen Current (WSC) core (averaged over the three easternmost Fram Strait moorings) at different depths in FESOM historical simulation and mooring observations. The Fram Strait mooring observations are described by Beszczynska-Moeller et al. (2012) and von Appen et al. (2016). (c) Atlantic Water (AW, $> 2^{o}$C) volume transport in the WSC in FESOM historical simulation and observations. The observed volume transport and the argument for the temperature threshold of the AW are provided by Beszczynska-Moeller et al. (2012). (d) The annual mean AW volume transport in the WSC in FESOM historical simulation in the studied period (2000-2019). The correlation coefficients between the FESOM results and observations are shown in (a)(b)(c) for both monthly and annual mean time series.

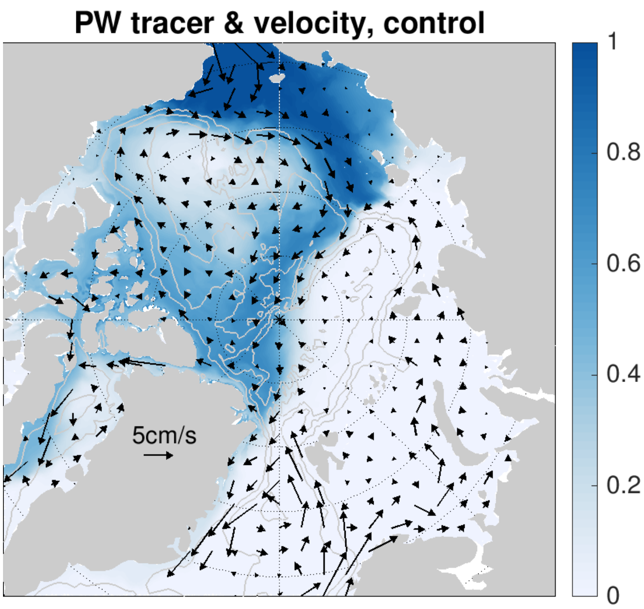

Figure S3. Pacific Water passive tracer concentration [color] and ocean velocity [vectors] averaged over the upper 150 m in the control simulation used in Section 2. It is the model result when wind perturbations are not applied, in contrast to Figure 4J-L.

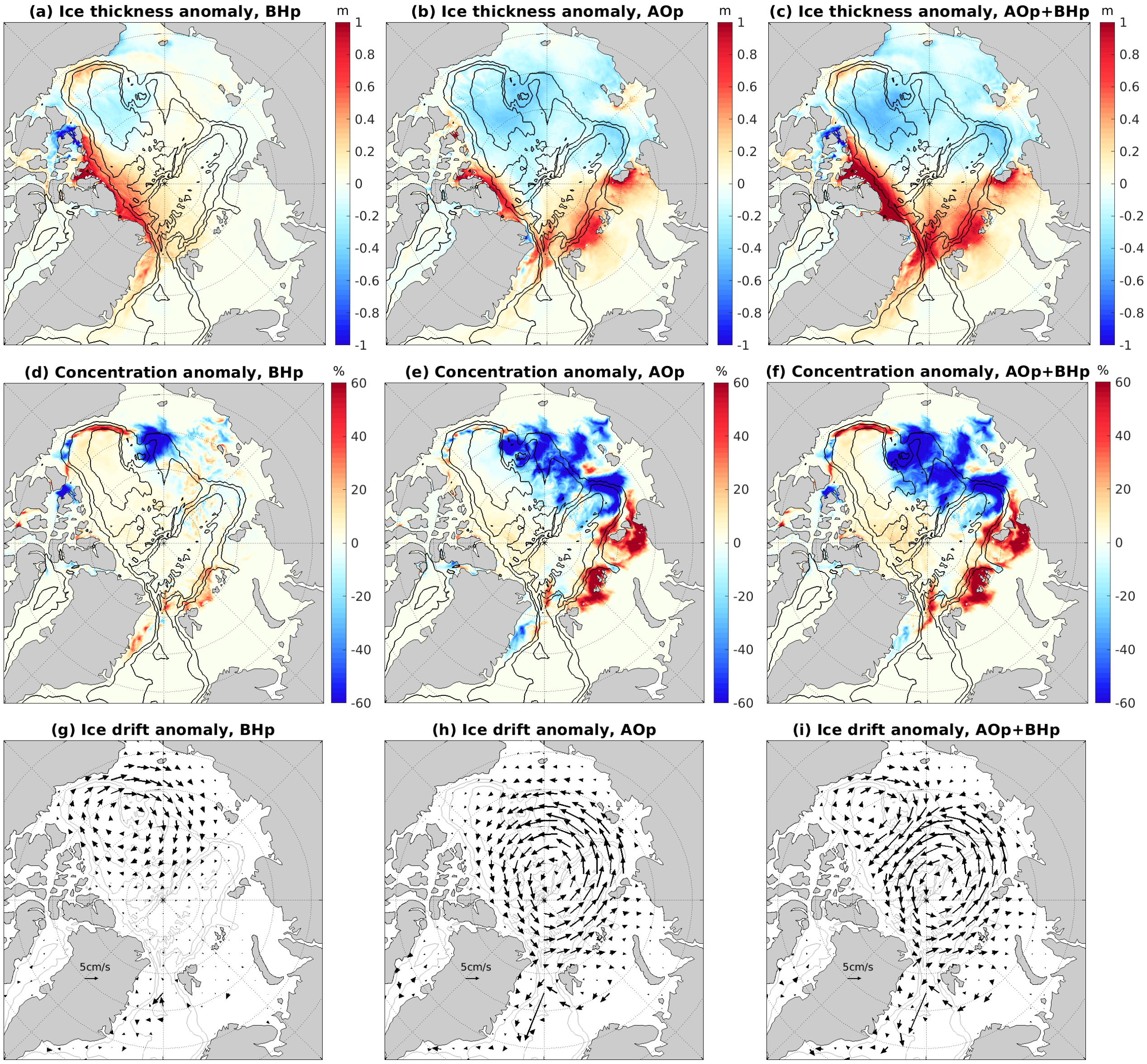

Figure S4. (a) Difference of annual mean sea ice thickness between the positive Beaufort High (BH) perturbation experiment and the control run (former minus latter). (d) Difference of September sea ice concentration between the positive BH perturbation experiment and the control run. (g) Difference of March sea ice drift between the positive BH perturbation experiment and the control run. (b)(e)(h) The same as (a)(d)(g), but for the positive Arctic Oscillation (AO) perturbation experiment. (c)(f)(i) The same as (a)(d)(g), but for the positive AO plus positive BH perturbation experiment.

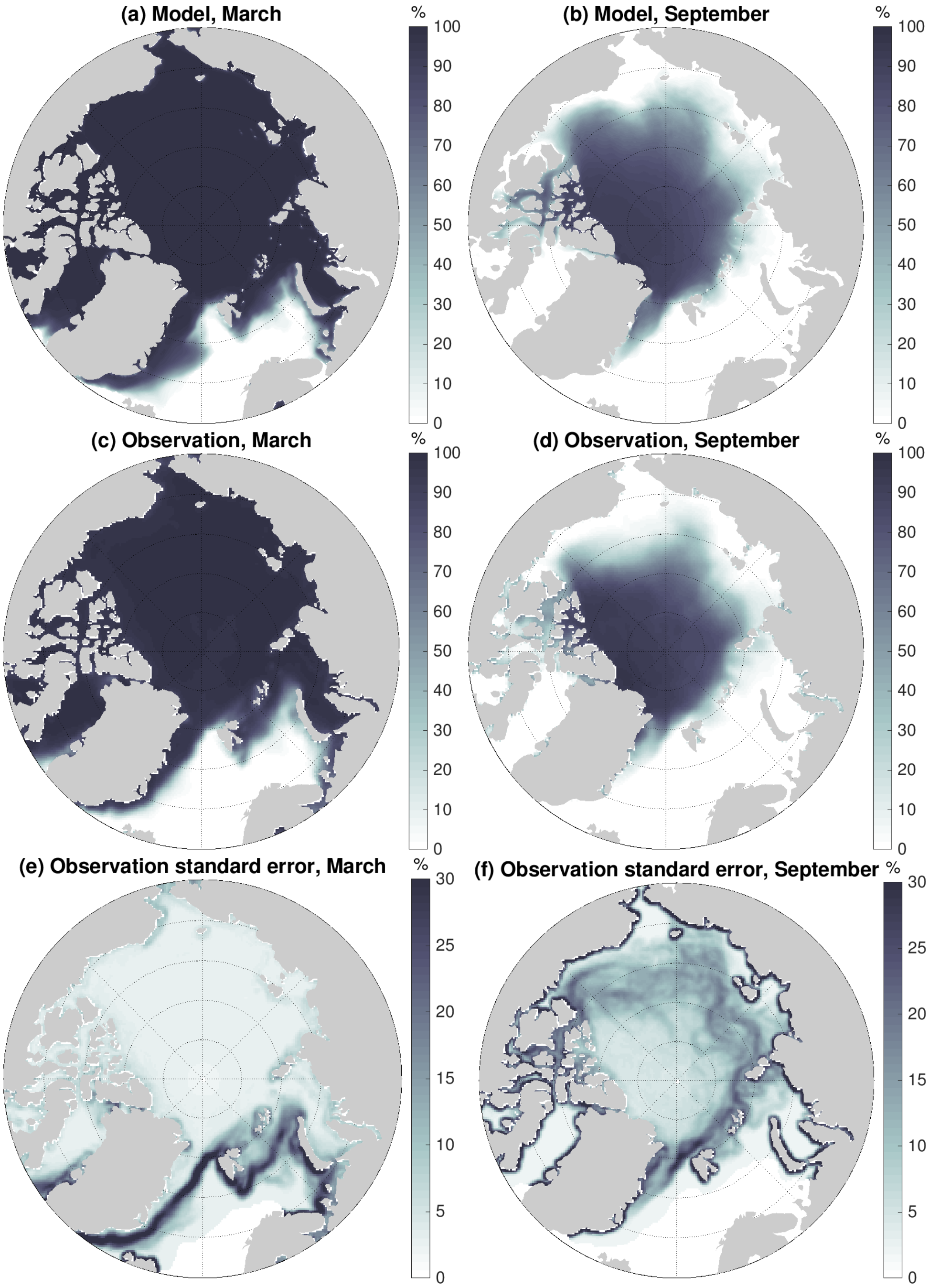

Figure S5. (upper) Simulated sea ice concentration in (a) March and (b) September in the FESOM historical simulation. (middle) OSI-SAF observed sea ice concentration in (c) March and (d) September. The average over 2000-2019 is shown. The observational uncertainty is shown in (e) for March and (f) for September. Observation reference: Lavergne, T., Sørensen, A. M., Kern, S., Tonboe, R., Notz, D., Aaboe, S., Bell, L., Dybkjær, G., Eastwood, S., Gabarro, C., Heygster, G., Killie, M. A., Brandt Kreiner, M., Lavelle, J., Saldo, R., Sandven, S., and Pedersen, L. T.: Version 2 of the EUMETSAT OSI SAF and ESA CCI sea-ice concentration climate data records, The Cryosphere, 13, 49-78, 2019.

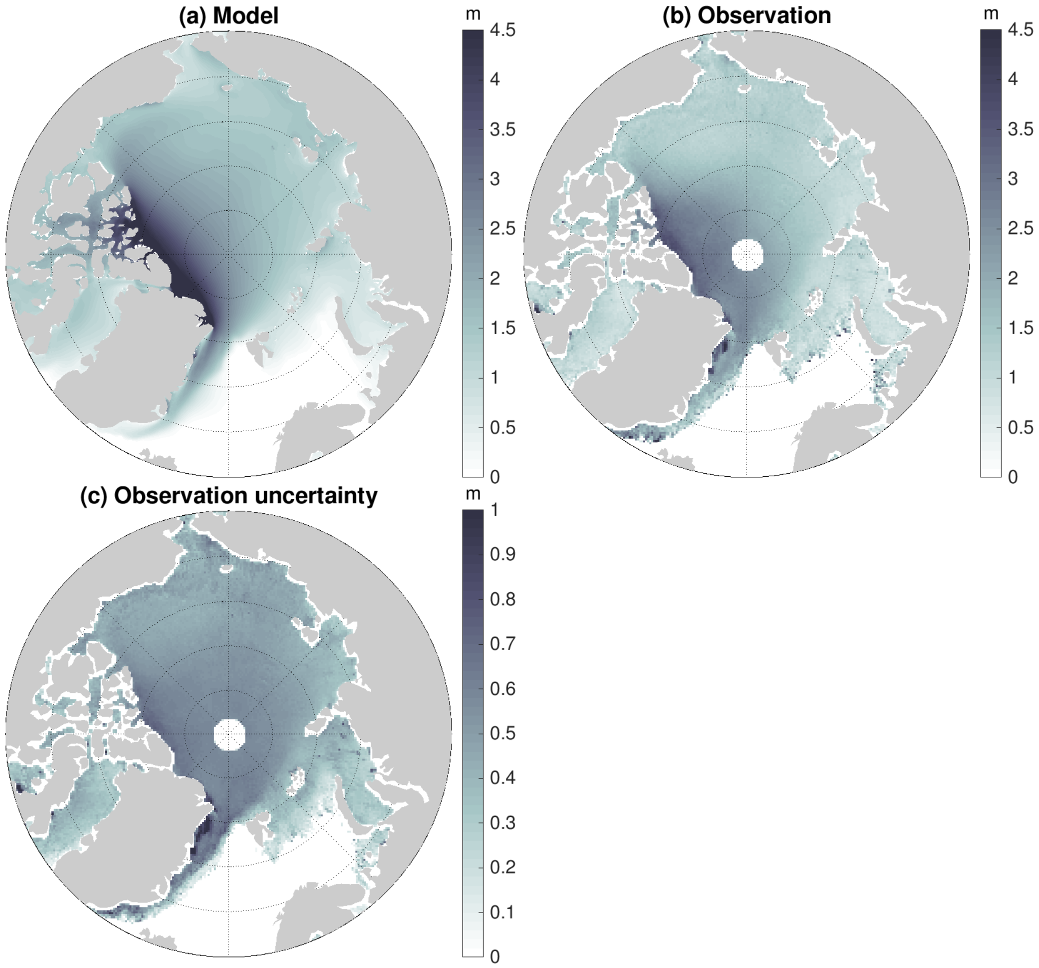

Figure S6. (a) FESOM simulated and (b) CryoSat-2 observed sea ice thickness averaged over months with observations available (October to April) from 2011 to 2019. (c) The CryoSat-2 observation uncertainty. Observation reference: Hendricks, S. and Ricker, R. (2019): Product User Guide and Algorithm Specification: AWI CryoSat-2 Sea Ice Thickness (version 2.2).

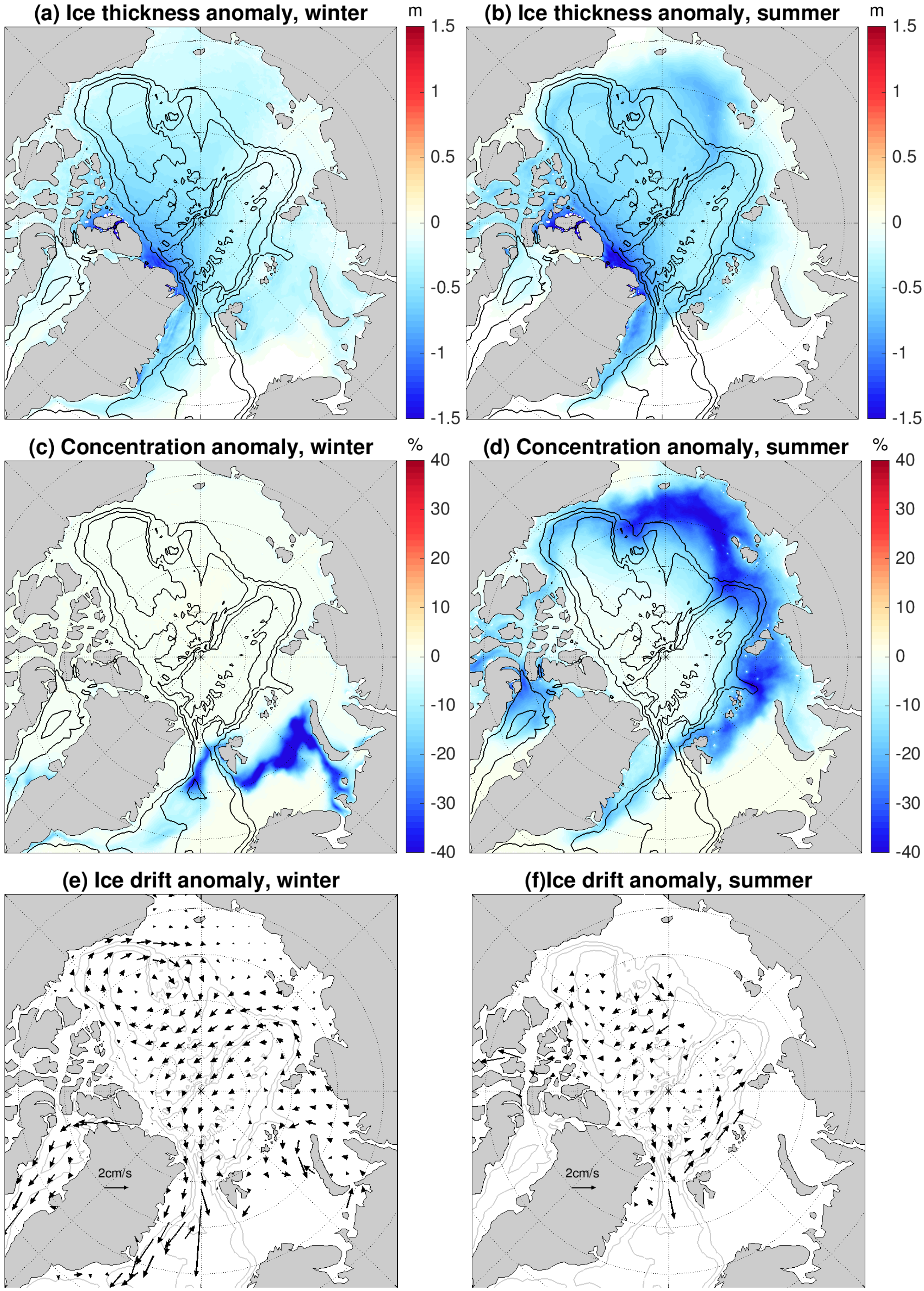

Figure S7. (a) Difference of winter sea ice thickness between the historical simulation and wind_vari simulation (former minus latter). (b) The same as (a), but for summer. (c)(d) The same as (a)(b), but for sea ice concentration. (e)(f) The same as (a)(b), but for sea ice drift.

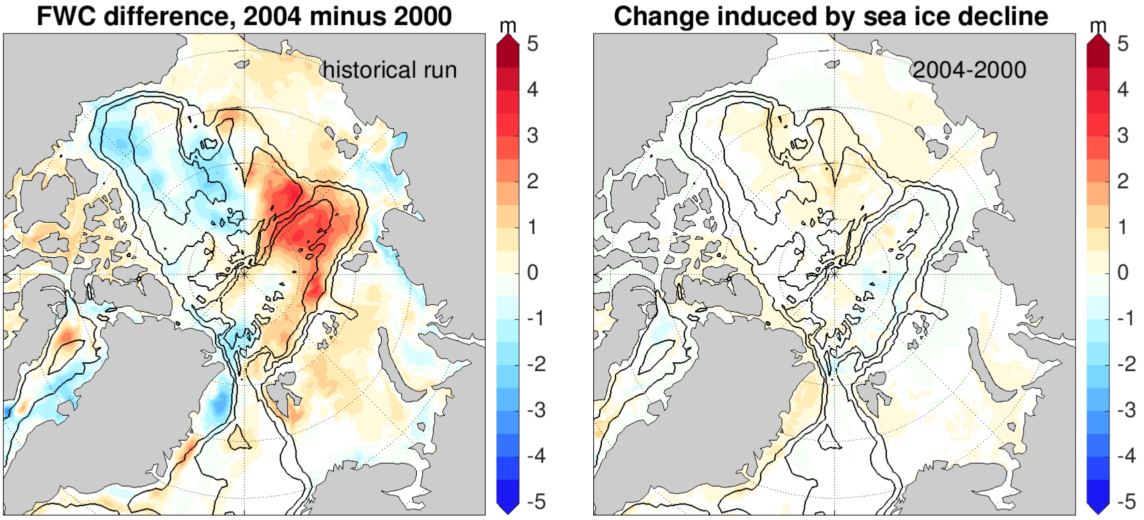

Figure S8. (left) Change in freshwater content (FWC, m) from 2000 to 2004 in the historical simulation. (right) The FWC change due to sea ice decline in this period.

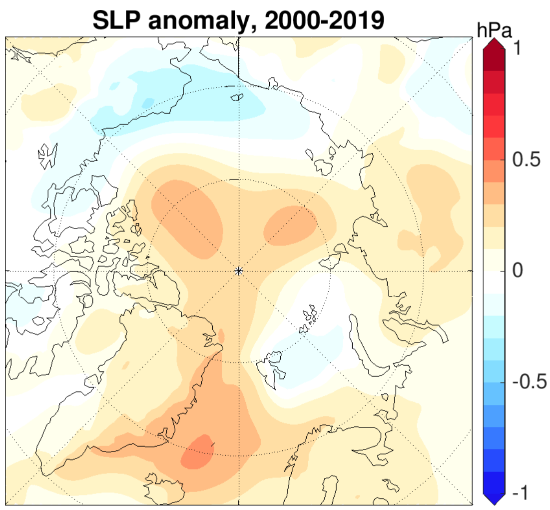

Figure S9. The anomaly of sea level pressure (SLP) in the period 2000–2019.